This is a preprint, the final version is subject to change, of the American Mineralogist (MSA)
Cite as Authors (Year) Title. American Mineralogist, in press.
(DOI will not work until issue is live.) DOI: http://dx.doi.org/10.2138/am-2017-6180

**Revision 1**

# Extraterrestrial formation of oldhamite and portlandite through thermal metamorphism of calcite in the Sutter's Mill carbonaceous chondrite

Christopher W. Haberle [1] and Laurence A. J. Garvie [1,2]

[1]School of Earth and Space Exploration, Arizona State University, Tempe, Arizona 85287, USA

[2]Center for Meteorite Studies, Arizona State University, Arizona 85287-6004, USA

## Abstract

The CM and CI carbonaceous chondrites are typically dominated by phyllosilicates with variable proportions of tochilinite, anhydrous silicates, carbonates, sulfides, sulfates, oxides and organic compounds. During thermal metamorphism the phyllosilicates dehydrate and decompose yielding water and olivine/enstatite. The thermal transformation of carbonate is less well understood, especially in the presence of volatile decomposition products, such as CO, $CO_2$, $SO_2$, $H_2S$, and $H_2O$. Here is described the mineralogical transformation of calcite ($CaCO_3$) to oldhamite (CaS) and portlandite ($Ca(OH)_2$) during extraterrestrial thermal metamorphism on the Sutter's Mill parent body. Sutter's Mill is a regolith breccia consisting of at least two lithologic components: phyllosilicate-calcite-bearing and anhydrous olivine-rich. Evidence suggests that the anhydrous stones were derived from extraterrestrial heating of the phyllosilicate-calcite-bearing material. One of only three Sutter's Mill stones (SM3) collected prior to heavy rainfall over the recovery site is the focus of this study. Its powder X-ray diffraction patterns are dominated by olivine, with lesser enstatite, Fe-sulfides, magnetite, and oldhamite. Oldhamite is

absent in the rained-on stones reflecting its water sensitivity and the pristine nature of SM3. Optical micrographs show whitish to bluish grains of oldhamite and portlandite embedded in dark, fine-grained matrix. The presence of abundant olivine and absence of phyllosilicates, tochilinite, and carbonate indicates that SM3 underwent heating to ~ 750 °C. At this temperature, calcite would have decomposed to lime (CaO). Volatilization experiments show that CO, $CO_2$, $SO_2$, and $H_2S$ evolve from CM and CI chondrites heated above 600 °C. Lime that formed through calcite decomposition would have reacted with these gases forming oldhamite under reducing conditions. Residual lime not converted to oldhamite, would have readily hydrated to portlandite, possibly through retrograde reactions during cooling on the parent body. These reactions have parallels to those in coal-fired electricity generating plants and provide an analogous system to draw comparison. Furthermore, the identification of these minerals, which are sensitive to terrestrial alteration, and determination of their formation is enabled only by the rapid collection of samples from an observed fall and their subsequent curation.

K**eywords**: Sutter's Mill, portlandite, oldhamite, dehydration, dehydroxylation, sulfidation, thermal metamorphism, carbonaceous chondrite

## Introduction

Carbonaceous chondrites represent primitive Solar System materials with chemical similarities to that of the solar photosphere (Anders and Grevesse 1989). Many of the CM and CI carbonaceous chondrites are water-rich and contain a suite of organic compounds making them central to the study of the origins of life. Investigations of the aqueous and thermal evolution of these primitive objects is important to understanding their role in planetary formation and the distribution and composition of volatile species and organic material in the Solar System.

Aqueous alteration of early Solar System materials modifies their mineralogy and petrology through hydration of anhydrous silicates forming phyllosilicates, alteration of Fe-Ni metal, and precipitation of carbonates and sulfates (McSween 1979; Tomeoka and Buseck 1985; Browning et al. 1996; Rubin et al. 2007). Additionally, aqueously altered carbonaceous chondrites can experience thermal metamorphism, acting to dehydrate, decompose, and reduce minerals and organic compounds (Gibson et al. 1972, 1974a, 1974b; Tomeoka et al. 1989a; Nozaki et al. 2006; Court and Sephton 2014; Tonui et al. 2014; Pizzarello and Garvie 2014; Court and Tan 2016). The energy driving this metamorphism can be generated by a range of processes including decay of short-lived radioisotopes, transient impact-generated thermal pulses, or orbital conditions that draw the parent body close to the Sun.

Thermal metamorphism of the CM and CI carbonaceous chondrites leads to dehydration of phyllosilicates, pyrolysis of organic compounds, and decomposition of tochilinite, carbonates, and sulfates. This heating releases a variety of gases, such as $SO_2$, $H_2S$, $H_2$, $H_2O$, COS, $CS_2$, $CO_2$, CO, and $CH_4$, which can react with the residual phases (Gibson et al. 1972, 1974a, 1974b; Burgess et al. 1991; Court and Sephton 2014; Court and Tan 2016). Knowledge of these

decomposition products and residual phases is important for understanding the processes that alter primitive bodies and is relevant to in situ resource utilization, given the recent interest in asteroidal materials as sources of raw materials (e.g., Lewis et al. 1993; Elvis 2013; Rabade et al. 2016). Several CM carbonaceous chondrites show mineralogies and textures indicative of a thermally metamorphosed phyllosilicate-rich precursor, such as Belgica 7904, Yamato 86720, Dhofar 225, and Dhofar 735 (Tomeoka et al. 1989a; Tomeoka 1990; Ivanova et al. 2010). Only two CI carbonaceous chondrites, Yamato 86029 and Yamato 82162, show mineralogical evidence for post-hydration thermal metamorphism (Tomeoka et al. 1989b; Tonui et al. 2003). These heated meteorites are natural laboratories providing insight into the products and mechanisms of thermal metamorphism on the CM and CI carbonaceous chondrite parent bodies. All previous examples of thermally metamorphosed CM and CI carbonaceous chondrites are finds, and hence have experienced terrestrial weathering. However, Sutter's Mill is a recent fall; this meteorite is mineralogically and isotopically similar to the CM chondrites (Jenniskens et al. 2012), but many of the stones appear to have been extraterrestrially heated following hydration (Garvie 2013). Thus, study of this meteorite provides insight into extraterrestrial thermal metamorphism of CM carbonaceous chondrites sans terrestrial weathering.

Sutter's Mill fell on April 22$^{nd}$, 2012 over the northern Sierra Nevada foothills (Fries et al. 2014). Approximately 90 stones were recovered, with a cumulative mass of ~1 kg (Jenniskens et al. 2012). Each stone is given an alphanumeric tag beginning with SM (Sutter's Mill) followed by an incremental number. The first three stones (SM1-SM3) were collected on April 24$^{th}$, 2012, before heavy rain fell across the recovery area. This investigation focuses on pre-rain stone SM3, with comparisons to SM2 (pre-rain) and SM41.

Sutter's Mill is a regolith breccia classified as a carbonaceous chondrite with no additional petrologic type or group association (Jenniskens et al. 2012; Garvie 2013; Zolensky et al. 2014). The $\delta^{18}O$ isotopes partially overlap the CM2 field and the $^{54}Cr$ excesses overlap that of Murchison (CM2) suggesting a CM-like composition (Ziegler and Garvie 2013; Yamakawa and Yin 2014). Bulk mineralogical observations of seven stones (SM3, 6, 8, 38, 41, 49, and 65) revealed two lithologic components: anhydrous olivine-rich and phyllosilicate-calcite-bearing (Garvie 2013). The phyllosilicate-calcite-bearing stones show broad X-ray reflections indicative of smectite-group minerals, whereas reflections for serpentine are of variable intensity and weak. These clay characteristics differ from the typical serpentine-dominated CM2 meteorites. The mineralogy of the olivine-rich SM stones is similar to that of Belgica 7904 that was heated extraterrestrially to >500 °C (Stage III and IV in Nakamura 2005). Sutter's Mill adds to an increasing number of CM and CI carbonaceous chondrites found to have experienced a range of thermal metamorphic conditions on their parent bodies (Tomeoka, 1990; Nakamura 2005; Ivanova et al. 2010; Tonui et al. 2014).

Sutter's Mill is the only carbonaceous chondrite known to host oldhamite (CaS) (Jenniskens et al 2012; Garvie 2013; Zolensky et al. 2014), a mineral typical of the enstatite chondrites and aubrites (Rubin 1997). Under reducing conditions oldhamite is predicted to condense from a nebular gas, consistent with its presence in enstatite chondrites (Larimer and Bartholomay 1979, Grossman et al. 2008). It has also been proposed to form from Fe-poor chondrule melts with moderate S concentrations (Piani et al. 2016). Therefore, its occurrence in the more oxidized Fe-rich carbonaceous chondrites is unexpected. Two previous studies have identified oldhamite within SM2 and SM3 (Garvie 2013; Zolensky et al. 2014), with Zolensky et al. (2014) suggesting its presence due to physical mixing with an E-type asteroid on the Sutter's

Mill parent body. Physical mixtures of chondritic material are not an undocumented occurrence and there are well-characterized examples e.g., Kaidun and Almahata Sitta (Zolensky and Ivanov 2003; Zolensky et al. 2010). Here we propose a reaction sequence for the in situ formation of oldhamite and portlandite from calcite during thermal metamorphism. Meteoritic portlandite has only been previously described as a terrestrial weathering product of oldhamite within the Norton County enstatite achondrite (Okada et al. 1981). We report on the first identification of indigenous meteoritic portlandite.

## Materials and Analytical Methods

This investigation focuses on SM3, with comparative observations from SM41 and a fragment of SM2. SM3 is a 5.0 g fusion crusted stone found April 24$^{th}$, 2012, before heavy rain fell over the fall site. Extensive measures were taken to minimize atmospheric and preparation contamination of the samples. The stone was split with a rock splitter and a ~3- x 5-mm chip was prepared and polished without the use of water. All SM3 pieces have been stored under a nitrogen atmosphere, and removed only for analysis. SM2 is a pre-rain stone found April 24$^{th}$, 2012. This stone was crushed by a car tire in a parking lot: here is studied a 30-mg fragment from the total ~4 g recovered. SM41 is a 9.3 g stone found May 4$^{th}$, 2012.

The samples were analyzed at the University of Arizona's Michael J. Drake Electron Microprobe lab with a CAMECA SX100 electron microprobe with five Wavelength Dispersive Spectrometers (WDS), and a Princeton Gamma-tech 5000 Energy Dispersive Spectrometer (EDS). Backscattered electron (BSE) imaging, EDS, and WDS analyses were used to determine the elemental compositions of the samples. WDS element maps were acquired for Ca, Fe, Mg, P, Si, Al, Cl, Ni, Na, and S.

Powder X-ray diffraction (XRD) patterns were acquired with a Rigaku MiniFlex 600 diffractometer, with a post-diffraction monochromator, employing Cu Kα radiation. Data were acquired from 2 to 65° at 0.02° steps, and 60 s/step. XRD samples were prepared from ~10 mg chips (~2 mm piece). The chips were crushed and mixed with a few mL of dry methanol. The resulting slurry was pipetted and spread into a thin, smooth film on a low-background single-crystal quartz plate. This slurry was dried rapidly (~ 5 s) under flowing warm air forming a thin film. Selected samples were also prepared as a dry powder deposited directly onto the quartz plate: no differences were seen between patterns from the two preparation methods showing that the methanol did not affect the water-sensitive minerals.

Thermogravimetric (TG) data was acquired under flowing He from 20° to 1000° C, with a heating rate of 10°C/min. Sample sizes were ~40 mg. Data were acquired from three separate chips of SM3, and for comparison from SM41, Murchison (CM2), and Orgueil (CI1).

Raman point spectra were acquired over low- (130-2500 $cm^{-1}$) and high-wavenumber (3400-3800 $cm^{-1}$) spectral ranges, with exposure times of 1 and 10 s, respectively. A laser power of 3 mW and λ=532 nm excitation was employed in both spectral regions. Micro-Raman mapping was conducted using a HORIBA Jobin Yvon Scientific XploRA dispersive confocal micro-Raman spectrometer with a laser excitation of λ=532 nm. Prior to analysis the sample was ground slightly and polished to expose a fresh surface.

## Results

Petrographic observations of SM3 show rounded, light-colored clasts and chondrules (some with fine-grained rims) embedded in dark, fine-grained matrix (Fig. 1a, S1). Irregularly shaped 10 to 250 μm bluish-white grains are distributed throughout the matrix (Fig. 1a,b, S1):

158 these grains are Ca-rich (Fig. 1d, S2). Many of the Ca-rich grains are also S-rich, with below
159 detectable levels of other metals (Fig. 1c, S2). These Ca-S-rich grains are uniformly distributed
160 across much of the polished mount (area ~1 $cm^2$; Fig. S1). Some grains are embedded in the
161 light-colored olivine-rich clasts, whereas many are in the matrix. Larger Ca-rich grains often
162 have S-rich exteriors and S-free cores (Fig. 1c, 2). In addition to Ca, WDS and element mapping
163 show that the S-free cores are O-rich, with minor Cl (Ca:O ratio near 0.44 and ~2 wt% Cl). The
164 Ca-O-rich cores are exceedingly electron-beam sensitive. The two largest grains (~200 μm
165 across) are rimmed: one with olivine and the other Fe-Ni sulfide (Fig. 2, S2). These grains are
166 the only ones observed with this petrographic relationship and are also observed through
167 computed tomography scans (Ebel and Hill 2012; Jenniskens et al. 2012). The WDS maps show
168 that Cl is largely associated with the Ca-O-rich cores at the ~2 wt% level, with a few grains
169 displaying higher concentrations (bright blue grain arrowed in Fig. S1). Chlorine correlates with
170 Ca, and is not associated with higher concentrations of other metals such as Na, K, or Mg.
171 SM41 is similar in appearance to SM3 (Fig. 3), with rounded, light-colored clasts and
172 chondrules embedded in dark fine-grained matrix. Irregularly shaped white grains of calcite 10-
173 300 μm in size are distributed uniformly across the sample. Calcium and S element distributions
174 are not correlated, revealing the absence of Ca-S-bearing grains.
175 The SM3 powder XRD patterns are dominated by intense, broad reflections from olivine,
176 with less-intense reflections from Fe-sulfides (pentlandite, troilite), magnetite, oldhamite, and
177 traces of enstatite. Absent are the 13.5 Å and 7.3 Å 001 basal reflections characteristic of
178 smectite and serpentine clays, respectively. A large (150 μm), altered Fe-Ni metal grain was also
179 identified through petrographic and electron microprobe analysis (Haberle et al. 2014). Relative
180 to the dominant olivine phase, the XRD patterns from five separate ~2-mm-sized SM3 chips are

similar, with minor intensity differences reflecting small variations in the non-olivine components. The powder pattern from SM2 is similar to that from SM3, showing oldhamite reflections and higher intensity reflections for enstatite. In comparison, SM41 is dominated by reflections from phyllosilicates and a large amorphous contribution, with lesser Fe-sulfides, calcite, magnetite, olivine, and enstatite. No oldhamite or Ca sulfate was detected by XRD. Also absent from SM41 are reflections from tochilinite, a common mineral in CM2 chondrites.

Heated to 1000 °C, the TG data from SM3 show mass loss of 2.5 wt%, whereas SM41 has mass loss of 11.4 wt%. The SM stones exhibit low mass losses compared to CM and CI carbonaceous chondrites, for instance, Murchison (CM2) and Orgueil (CI1) experienced losses of 15 wt% and 22 wt%, respectively.

Raman spectra from the large Ca-rich grain in Figure 2b show bands at 356, 1080, 1331, 1583, and 3620 $cm^{-1}$ (Fig. 4). The sharp bands at 356 and 3620 $cm^{-1}$ correspond to the ν2 bending and ν1 OH stretching of $Ca(OH)_2$, respectively (Schmid and Dariz 2015). The weak Raman mode at 1080 $cm^{-1}$ corresponds to the ν1 C-O stretching mode of calcite (Schmid and Dariz 2015; Ševčík et al. 2016). The broad modes at 1350 and 1580 $cm^{-1}$ match those of the disordered carbon (D) and graphite (G) Raman active modes present in a variety of carbonaceous materials (Bonal et al. 2006; Quirico et al. 2009).

The powder XRD data show that SM3 contains abundant oldhamite. WDS data show multiple dispersed Ca-S-rich grains consistent with oldhamite. The largest grains have S-free, Ca-O-rich cores, with Raman data consistent with portlandite.

## Discussion

### Evidence for indigenous oldhamite and portlandite

The XRD, Raman, and elemental data show the presence of oldhamite and portlandite; both are moisture sensitive. The occurrence of oldhamite in the olivine-rich pre-rain stones (SM2 and 3) and absence in the olivine-rich rained-on stones (Garvie 2013; Zolensky et al., 2014) shows the ease with which this mineral is altered by water and speaks to the minimal terrestrial contamination of SM3. The presence of portlandite can be explained as either terrestrial alteration or as indigenous to SM3. In the former case, portlandite would have formed through terrestrial hydration of extraterrestrial lime (CaO). We consider this unlikely, as SM3 was not exposed to rain. In addition, the olivine-rich pre-rain stones (SM2 and 3) are unlike other CM-like carbonaceous chondrites in being very hard and sintered (also noted by Zolensky et al. 2014), thus limiting the exposure of interior surfaces to atmospheric moisture. Also, hydration of lime would have led to volume expansion as portlandite has a molar volume (33.08 $cm^3$/mol) twice that of lime (16.79 $cm^3$/mol) (Kudłacz and Rodriguez-Navarro 2014). Evidence of this expansion would be apparent on a cut surface and has not been observed on the prepared specimens. These lines of evidence are consistent with the portlandite being indigenous to SM3.

**Sutter's Mill lithologies**

The Sutter's Mill fall is unusual in that it consists of stones with olivine-rich and phyllosilicate/amorphous-rich mineralogies. Only one of the stones previously studied, SM8, is olivine-rich and shows weak phyllosilicate reflections (Garvie 2013). The bulk $\delta^{18}O$ value of the phyllosilicate-rich stones is 13-18‰ and overlaps that of the olivine-rich stones, which span 11-27‰ (Ziegler and Garvie 2013). These data overlap with the CM field, but are also $^{16}O$-poor extending to values of the metamorphosed CM-like chondrites (Ivanova et al. 2010). Given the petrographic, though not mineralogical, similarities between the hydrated and anhydrous stones

(Figs. 1 and 3), and the oxygen isotopic data, we suggest that they are genetically related. In this scenario, the anhydrous SM3 derives from SM41-like material through in-situ thermal metamorphism on the Sutter's Mill parent body.

**Evidence for thermal metamorphism of SM3**

SM3 shows low mass loss during TG analysis (2.5 wt%), with its mineralogy dominated by olivine, with an absence of phyllosilicates. Thermally metamorphosed CM carbonaceous chondrites, such as Belgica 7904 (Tomeoka 1990), Yamato 86720 (Tomeoka et al. 1989a), Dhofar 225 and Dhofar 735 (Ivanova et al. 2010), are also olivine-rich with low water contents. It has been posited (Tomeoka et al. 1989a; Tomeoka 1990; Ivanova et al. 2010) that these stones experienced extraterrestrial thermal metamorphism that dehydrated phyllosilicates leading to recrystallization of olivine and minor enstatite (Brindley and Hiyami 1965; Akai 1992). The XRD profiles of recrystallized secondary olivine exhibit broad diffraction peaks that are distinct from the sharp reflections of primary olivine (Nakamura 2005). The olivine diffraction peaks in SM3 are similarly broad consistent with secondary olivine that recrystallized from matrix phyllosilicates. The temperature required to initiate this reaction is ~400° C, with complete dehydroxylation and recrystallization to olivine occurring at ~750° C (Brindley and Hiyami 1965; Akai 1990,1992; Nakamura 2005; Ivanova et al. 2010; Tonui et al. 2014).

**Thermal metamorphism of calcite to oldhamite and portlandite**

Calcite is common in CM chondrites and is also present in SM41 (Johnson and Prinz 1993; Garvie 2013). We propose that calcite originally present in SM3 was calcined to lime. The calcination reaction is endothermic and decomposition typically initiates above 600° C

(Rodriguez-Navarro et al. 2009; Galan et al. 2013), though can begin ~400 °C (Wang and Thomson 1995). Various factors, related to the physical properties of the material and partial pressure of $CO_2$, influence the initiation temperature and rate of reaction but, in general, higher temperature favors the forward reaction (Stanmore and Gilot 2005). The kinetics of the calcination reaction is thoroughly studied, as it is a reaction frequently utilized in a number of industrial processes.

Lime is commonly employed as a sorbent to capture sulfur emissions from coal-fired electricity-generating plants and this can lead to the formation of oldhamite under reducing conditions (Hansen et al. 1993; Agnihotri et al. 1999). There are two similar reactions that induce oldhamite formation, both utilize lime to react with S-bearing gases ($SO_2$ and $H_2S$; Hansen et al. 1993; Agnihotri et al. 1999); these gases are also common volatile products of heated CM and CI carbonaceous chondrites (Gibson et al. 1972, 1974a,1974b; Court and Sephton 2014; Court and Tan 2016). For example, upon heating to 1000°C, Murray (CM2), Murchison (CM2), and Orgueil (CI1) release $SO_2$, with a trimodal release pattern with peaks located at ~250°C, 400-500 °C, and 600-800 °C. Murray and Orgueil also exhibit release of $H_2S$ at ~450°C, with Murray showing additional release >800°C (Gibson et a. 1972, 1974a, 1974b).

At high temperature lime reacts with $SO_2$ to form CaS or $CaSO_4$ depending upon the reducing potential $P_{CO}/P_{CO_2}$ of the system (Oh and Wheelock 1990; Hansen et al. 1993). When the reducing potential is elevated (>0.2), the formation of oldhamite is favored through:

$$CaO + SO_2 + 3CO \rightarrow CaS + 3CO_2$$

Alternatively, above 700°C with > 2000 ppm $H_2S$, oxide sulfidation of CaO will occur through:

$$CaO + H_2S \rightarrow CaS + H_2O$$

Both reactions form oldhamite along the exterior of the grain with a reaction front propagating inward. In SM3, grains smaller than ~50 μm have been completely converted to oldhamite, while larger grains retain a core of lime (Fig. 1, 2, S2).

The residual interior lime is extremely hygroscopic and readily forms portlandite when exposed to water vapor (Dubina et al. 2011, 2013). Following the event that heated SM3, cooling could have resulted in retrograde hydration of lime to portlandite. Furthermore, in the presence of steam and $CO_2$, evidence suggests that portlandite can be stable well above its dehydration temperature (~450 °C) as a transient or intermediate phase during calcination and sulfidation (Wang et al. 2010; Materić et al. 2015). This high temperature stability suggests that any lime formed, which was not converted to oldhamite, could persist as portlandite.

The two largest oldhamite-portlandite grains have rims of olivine and Fe-Ni sulfide (Fig. 2). The CM chondrites, and several SM stones, contain calcite grains with rims, such as Mg-rich serpentine, serpentine-tochilinite, cronstedtite, Fe sulfides, and an unidentified O-S-Fe mineral (de Leuw et al. 2010; Lee et al. 2014; Zolensky et al. 2014; Fujiya et al. 2015). The rims surrounding type 1a calcite in CM chondrites (Fig. 8 in Lee et al. 2014) show textural similarities to the rims we observe in Figure 2c. We suggest that the rims we observe are the thermally metamorphosed equivalent to rims surrounding calcite grains in CM chondrites. In SM3, these rimmed grains are rare but they provide additional supporting evidence that the abundant oldhamite grains were calcite prior to thermal metamorphism and are not xenocrysts from an enstatite chondrite or aubrite.

## Implications

295 Formation of oldhamite and portlandite through thermal processing of CM carbonaceous
296 chondrites presents a new understanding of the mineralogical transformations occurring on
297 carbonaceous chondrite parent bodies. The formation of oldhamite is commonly observed in
298 fluidized bed combustion (FBC) reactors, where crushed limestone is added to coal-fired reactors
299 to reduce sulfur emissions. In addition to oldhamite, FBC ash typically contains large quantities
300 of lime and portlandite revealing that it is a common end-product in high temperature
301 combustion processes involving calcite and carbonaceous materials, such as coal. Gas-solid
302 reactions used industrially for power generation and emission reduction have a parallel with
303 heated CM carbonaceous chondrites, and allow for the presence of portlandite and the reduced
304 phase oldhamite without the need to invoke physical mixing of reduced enstatite chondrites or
305 aubrites on the parent body. In addition, this study introduces portlandite as an indigenous
306 meteoritic mineral.

307 Moreover, these results underline the importance of studying fresh meteorite falls and the
308 need for their appropriate long-term curation. Oldhamite has not been reported from
309 mineralogically similar chondrites e.g., Belgica 7904 (Tomeoka, 1990; Nakamura 2005). This
310 absence could be the result of its water sensitivity and rapid decomposition. This sensitivity is
311 illustrated by the presence of oldhamite in the two studied pre-rain, olivine-rich stones, SM2 and
312 SM3, but not in the post-rain, olivine-rich stones.

313 Mineral assemblages of thermally metamorphosed CM carbonaceous chondrites are
314 unique and can shed light into the processes that acted to modify primitive meteorite parent
315 bodies. Oldhamite generated within a carbonaceous chondrite can be a sensitive indicator of the
316 redox conditions asteroidal material was exposed to during thermal metamorphism. Lime,
317 portlandite, oldhamite, dehydrated phyllosilicates, and olivine each have characteristic spectral

features that could be identified by the payload suites of the two sample collecting spacecraft currently travelling to suspected carbonaceous chondrites (OSIRIS-REx and Hayabusa II). As such, the identification and spatial distribution of these minerals on the surface of B- and C-type asteroids would be valuable for interpreting the thermal history of the materials exposed at the surface.

**Acknowledgments**

We thank Alan Rubin, Tasha Dunn and Steve Simon for constructive reviews greatly improving the clarity of this manuscript, Kenneth Domanik for his expertise and assistance with microprobe calibration and analysis, S.-H. Dan Shim, Kip Hodges and Alyssa Anderson for access and assistance with the collection of Raman spectra and maps, Jim Bell and the S.C.O.R.P.I.U.N. lab for the use of their XRD and the ASU Center for Meteorite studies for access to pristine samples. L.A.J.G was funded in part by NASA Emerging Worlds (EW) grant NNX17AE56G.

**References Cited**

Agnihotri, R., Chauk, S.S., Mahuli, S.K., and Fan, L.S. (1999) Mechanism of CaO reaction with $H_2S$: Diffusion through CaS product layer. Chemical Engineering Science, 54, 3443-3453.

Akai, J. (1992) TTT diagram of serpentine and saponite, and estimation of metamorphic heating degree of Antarctic carbonaceous chondrites. Antarctic Meteorite Research, 5, 120.

Akai, J. (1990) Mineralogical evidence of heating events in Antarctic carbonaceous chondrites, Y-86720 and Y-82162. Antarctic Meteorite Research, 3, 55.

340 Anders, E. and Grevesse, N. (1989) Abundances of the elements: Meteoritic and solar.
341 Geochimica et Cosmochimica Acta, 53, 197-214.
342 Bonal, L., Quirico, E., Bourot-Denise, M., and Montagnac, G. (2006) Determination of the
343 petrologic type of CV3 chondrites by Raman spectroscopy of included organic matter.
344 Geochimica et Cosmochimica Acta, 70, 1849-1863.
345 Brindley, G.W. and Hayami, R. (1965) Mechanism of formation of forsterite and enstatite from
346 serpentine. Mineralogy Magazine, 35, 189-195
347 Browning, L.B., McSween, H.Y., and Zolensky, M.E. (1996) Correlated alteration effects in CM
348 carbonaceous chondrites. Geochimica et Cosmochimica Acta, 60, 2621-2633.
349 Burgess, R., Wright, I.P., and Pillinger, C.T. (1991) Determination of sulphur - bearing
350 components in C1 and C2 carbonaceous chondrites by stepped combustion. Meteoritics,
351 26, 55-64.
352 Court, R.W. and Sephton, M.A. (2014) New estimates of the production of volatile gases from
353 ablating carbonaceous micrometeoroids at Earth and Mars during an E-belt-type Late
354 Heavy Bombardment. Geochimica et Cosmochimica Acta, 145, 175-205.
355 Court, R.W. and Tan, J. (2016) Insights into secondary reactions occurring during atmospheric
356 ablation of micrometeoroids. Meteoritics and Planetary Science, 51, 1163-1183.
357 de Leuw, S., Rubin, A.E., and Wasson, J.T. (2010) Carbonates in CM chondrites: Complex
358 formational histories and comparison to carbonates in CI chondrites. Meteoritics and
359 Planetary Science, 45, 513-530.
360 Dubina, E., Wadsö, L., and Plank, J. (2011) A sorption balance study of water vapour sorption
361 on anhydrous cement minerals and cement constituents. Cement and Concrete
362 Research, 41, 1196-1204.

Dubina, E., Korat, L., Black, L., Strupi-Šuput, J., and Plank, J. (2013) Influence of water vapour and carbon dioxide on free lime during storage at 80 C, studied by Raman spectroscopy. Spectrochimica Acta Part A: Molecular and Biomolecular Spectroscopy, 111, 299-303.

Ebel, D.S. and Hill, M. (2012) Computed Tomography (CT) of five samples of the Sutter's Mill CM2 chondrite. (Online). Available: http://digitallibrary.amnh.org/handle/2246/6408 (accessed July 7, 2016). American Museum of Natural History, New York, New York.

Elvis, M. (2013) Prospecting asteroid resources. In Asteroids: Prospective energy and material resources. P. 81-129 Springer Berlin Heidelberg.

Fries, M., Le Corre, L., Hankey, M., Fries, J., Matson, R., Schaefer, J., and Reddy, V. (2014) Detection and rapid recovery of the Sutter's Mill meteorite fall as a model for future recoveries worldwide. Meteoritics and Planetary Science, 49, 1989-1996.

Fujiya, W., Sugiura, N., Marrocchi, Y., Takahata, N., Hoppe, P., Shirai, K., Sano, Y., and Hiyagon, H. (2015) Comprehensive study of carbon and oxygen isotopic compositions, trace element abundances, and cathodoluminescence intensities of calcite in the Murchison CM chondrite. Geochimica et Cosmochimica Acta 161, 101-117.

Galan, I., Glasser, F.P., and Andrade, C. (2013) Calcium carbonate decomposition. Journal of Thermal Analysis and Calorimetry, 111, 1197-1202.

Garvie, L.A.J. (2013) Mineralogy of the Sutter's Mill Carbonaceous Chondrite. 44th Lunar and Planetary Science Conference, Abstract #2148.

Gibson, E.K. Jr. and Johnson, S.M. (1972) Thermogravimetric-quadrupole mass-spectrometric analysis of geochemical samples. Thermochimica Acta, 4, 49-56.

385 Gibson, E.K. Jr. (1974a) Inorganic gas release studies and thermal analysis investigations on
386 carbonaceous chondrites. Meteoritics, 9, 343-344.
387 Gibson, E.K., Moore, G.W., and Johnson, S.M. (1974b) Summary of analytical data from gas
388 release investigations, volatilization experiments, elemental abundance measurements on
389 lunar samples, meteorites, minerals, volcanic ashes and basalts. NASA L.B. Johnson
390 Space Center, Houston, Tex.
391 Grossman, L., Beckett, J.R., Fedkin, A.V., Simon, S.B. and Ciesla, F.J. (2008) Redox conditions
392 in the solar nebula: Observational, experimental, and theoretical constraints. Reviews in
393 Mineralogy and Geochemistry, 68, 93-140.
394 Haberle, C.W., Garvie, L.A.J, Domanick, K., and Christensen, P.R. (2014) Mineralogical
395 complexity of altered kamacite in Sutter's Mill (SM3, pre-rain): insights into asteroidal
396 dehydration. 45th Lunar and Planetary Science Conference, Abstract #2818
397 Hansen, P., Dam-Johansen, K., and Østergaard, K. (1993) High-temperature reaction between
398 sulphur dioxide and limestone—V. The effect of periodically changing oxidizing and
399 reducing conditions. Chemical Engineering Science, 48, 1325-1341.
400 Ivanova, M.A., Lorenz, C.A., Nazarov, M.A., Brandstaetter, F., Franchi, I.A., Moroz, L.V.,
401 Clayton, R.N., and Bychkov, A.Y. (2010) Dhofar 225 and Dhofar 735: Relationship to
402 CM2 chondrites and metamorphosed carbonaceous chondrites, Belgica-7904 and
403 Yamato-86720. Meteoritics and Planetary Science, 45, 1108-1123.
404 Jenniskens, P., Fries, M.D., Yin, Q.Z., Zolensky, M., Krot, A.N., Sandford, S.A., Sears, D.,
405 Beauford, R., Ebel, D.S., Friedrich, J.M., and Nagashima, K. (2012) Radar-enabled
406 recovery of the Sutter's Mill meteorite, a carbonaceous chondrite regolith breccia.
407 Science, 338, 1583-1587.

Johnson, C.A. and Prinz, M. (1993) Carbonate compositions in CM and CI chondrites and implications for aqueous alteration. Geochimica et Cosmochimica Acta, 57, 2843-2852.

Kudłacz, K. and Rodriguez-Navarro, C. (2014) The mechanism of vapor phase hydration of calcium oxide: implications for $CO_2$ capture. Environmental Science and Technology, 48, 12411-12418.

Larimer, J.W. and Bartholomay, M. (1979) The role of carbon and oxygen in cosmic gases: Some applications to the chemistry and mineralogy of enstatite chondrites. Geochimica et Cosmochimica Acta, 43, 1455-1466.

Lee, M.R., Lindgren, P., and Sofe, M.R. (2014) Aragonite, breunnerite, calcite and dolomite in the CM carbonaceous chondrites: High fidelity recorders of progressive parent body aqueous alteration. Geochimica et Cosmochimica Acta, 144, 126-156.

Lewis, J.S., McKay, D.S., and Clark, B.C. (1993) Using resources from near-Earth space. In Lewis J., Matthews M.S., Guerrieri M.L., Eds. Resources of Near-Earth Space, p.3-14, The University of Arizona Press, Tucson&London

Materić, V., Ingham, B., and Holt, R. (2015) In situ synchrotron XRD investigation of the dehydration and high temperature carbonation of $Ca(OH)_2$. CrystEngComm, 17, 7306-7315.

McSween, H.Y. (1979) Alteration in CM carbonaceous chondrites inferred from modal and chemical variations in matrix. Geochimica et Cosmochimica Acta, 43, 1761-1770.

Nakamura, T. (2005) Post-hydration thermal metamorphism of carbonaceous chondrites. Journal of the Mineralogical and Petrological Sciences, 100, 260-272.

Nozaki, W., Nakamura, T. and Noguchi, T. (2006) Bulk mineralogical changes of hydrous micrometeorites during heating in the upper atmosphere at temperatures below 1000 C. Meteoritics and Planetary Science, 41, 1095-1114.

Oh, J.S., and Wheelock, T.D. (1990) Reductive decomposition of calcium sulfate with carbon monoxide: reaction mechanism. Industrial and Engineering Chemistry Research, 29, 544-550.

Okada, A., Keil, K., and Taylor, G.J. (1981) Unusual weathering products of oldhamite parentage in the Norton County enstatite achondrite. Meteoritics, 16, 141-152.

Piani, L., Marrocchi, Y., Libourel, G., and Tissandier, L. (2016) Magmatic sulfides in the porphyritic chondrules of EH enstatite chondrites. Geochimica et Cosmochimica Acta, 195, 84-99.

Pizzarello, S. and Garvie, L.A.J. (2014) Sutter's Mill dicarboxylic acids as possible tracers of parent-body alteration processes. Meteoritics and Planetary Science, 49, 2087-2094.

Quirico, E., Montagnac, G., Rouzaud, J.N., Bonal, L., Bourot-Denise, M., Duber, S., and Reynard, B. (2009) Precursor and metamorphic condition effects on Raman spectra of poorly ordered carbonaceous matter in chondrites and coals. Earth and Planetary Science Letters, 287, 185-193.

Rabade, S., Barba, N., Garvie, L.A.J., and Thangavelautham, J. (2016) The case for solar thermal steam propulsion system for interplanetary travel: Enabling simplified ISRU utilizing NEOs and small bodies. 67th International Astronautical Congress, Abstract Code: IAC-16,D4,5,7,x34659

Rodriguez-Navarro, C., Ruiz-Agudo, E., Luque, A., Rodriguez-Navarro, A.B., and Ortega-Huertas, M. (2009) Thermal decomposition of calcite: Mechanisms of formation and textural evolution of CaO nanocrystals. American Mineralogist, 94, 578-593.

Rubin, A.E. (1997) Mineralogy of meteorite groups. Meteoritics and Planetary Science, 32, 231-247

Rubin, A.E., Trigo-Rodríguez, J.M., Huber, H., and Wasson, J.T. (2007) Progressive aqueous alteration of CM carbonaceous chondrites. Geochimica et Cosmochimica Acta, 71, 2361-2382

Schmid, T. and Dariz, P. (2015) Shedding light onto the spectra of lime: Raman and luminescence bands of CaO, $Ca(OH)_2$ and $CaCO_2$. Journal of Raman Spectroscopy, 46, 141-146.

Ševčík, R., Mácová, P., Sotiriadis, K., Pérez-Estébanez, M., Viani, A., and Šašek, P. (2016) Micro-Raman spectroscopy investigation of the carbonation reaction in a lime paste produced with a traditional technology. Journal of Raman Spectroscopy, 47, 1452-1457.

Stanmore, B.R. and Gilot, P. (2005) Review—calcination and carbonation of limestone during thermal cycling for CO 2 sequestration. Fuel Processing Technology, 86, 1707-1743

Tomeoka, K. and Buseck, P.R. (1985) Indicators of aqueous alteration in CM carbonaceous chondrites: Microtextures of a layered mineral containing Fe, S, O and Ni. Geochimica et Cosmochimica Acta, 49, 2149-2163.

Tomeoka, K., Kojima, H., and Yanai, K. (1989a) Yamato-86720: A CM carbonaceous chondrite having experienced extensive aqueous alteration and thermal metamorphism. In Proceedings of the NIPR Symposium on Antarctic Meteorites, 2, 55-74.

Tomeoka, K., Kojima, H., and Yanai, K. (1989b) Yamato-82162: A new kind of CI carbonaceous chondrite found in Antarctica. In Proceedings of the NIPR Symposium on Antarctic Meteorites, 2, 36-54.

Tomeoka, K. (1990) Mineralogy and petrology of Belgica-7904: A new kind of carbonaceous chondrite from Antarctica. Antarctic Meteorite Research, 3, 40.

Tonui, E., Zolensky, M., Lipschutz, M., Wang, M., and Nakamura, T. (2003) Yamato 86029: Aqueously altered and thermally metamorphosed CI-like chondrite with unusual textures. Meteoritics and Planetary Science, 38, 269-292

Tonui, E., Zolensky, M., Hiroi, T., Nakamura, T., Lipschutz, M.E., Wang, M.S., and Okudaira, K. (2014) Petrographic, chemical and spectroscopic evidence for thermal metamorphism in carbonaceous chondrites I: CI and CM chondrites. Geochimica et Cosmochimica Acta, 126, 284-306.

Wang, Y. and Thomson, W.J. (1995) The effects of steam and carbon dioxide on calcite decomposition using dynamic X-ray diffraction. Chemical Engineering Science, 50, 1373-1382.

Wang, C., Jia, L., Tan, Y., and Anthony, E.J. (2010) The effect of water on the sulphation of limestone. Fuel, 89, 2628-2632.

Yamakawa, A. and Yin, Q.Z. (2014) Chromium isotopic systematics of the Sutter's Mill carbonaceous chondrite: implications for isotopic heterogeneities of the early Solar System. Meteoritics and Planetary Science, 49, 2118-2127.

Ziegler, K. and Garvie, L.A.J. (2013) Bulk oxygen-isotope compositions of different lithologies in Sutter's Mill. 76th Annual Meteoritical Society Meeting, Abstract #5225.

494 Zolensky, M. and Ivanov, A. (2003) The Kaidun microbreccia meteorite: A harvest from the
495 inner and outer asteroid belt. Chemie der Erde-Geochemistry, 63, 185-246.
496 Zolensky, M., Herrin, J., Mikouchi, T., Ohsumi, K., Friedrich, J., Steele, A., Rumble, D., Fries,
497 M., Sandford, S., Milam, S. and Hagiya, K. (2010) Mineralogy and petrography of the
498 Almahata Sitta ureilite. Meteoritics and Planetary Science, 45, 1618-1637.
499 Zolensky, M., Mikouchi, T., Fries, M., Bodnar, R., Jenniskens, P., Yin, Q.Z., Hagiya, K.,
500 Ohsumi, K., Komatsu, M., Colbert, M., and Hanna, R. (2014) Mineralogy and
501 petrography of C asteroid regolith: The Sutter's Mill CM meteorite. Meteoritics and
502 Planetary Science, 49, 1997-2016.
503

504 **Figure 1.** Representative section of the SM3 polished mount showing the textural and chemical
505 relationship of clasts set in matrix. (**a**) Optical micrograph showing rounded tan-colored olivine,
506 brown Fe sulfide and whitish-blue grains in dark fine-grained matrix. (**b**) Modified optical image
507 showing the distribution of the whitish-blue grains of oldhamite and portlandite with all other
508 materials cropped. (**c**) Black and white map showing where these grains contain only Ca and S.
509 Pixels where Ca and S are both present above background values are set to 255 and appear white.
510 Pixels where other measured elements are present above background are set to a value of 0,
511 appearing black. This panel highlights the relationship of oldhamite with portlandite. (**d**) Ca
512 element distribution map showing WDS counts per pixel. Note the correlation with grains in (**b**)
513 and (**c**). Observe that the ~75μm whitish-blue grain in the upper right corner of the panel has an
514 even distribution of Ca in (**d**) but has an exterior rim of Ca and S in (**c**), as described in text.
515 Each panel in this figure covers the same area of the mount and the scale in (**a**) applies to all.
516

517 **Figure 2.** (**a** and **c**) False-color composite WDS x-ray element images highlighting petrographic
518 relationships of (**a**) oldhamite (Od) and portlandite (CH) and (**c**) rimming olivine (Ol) and
519 pentlandite (Pn). (**b**) Visible light image showing encased grains of portlandite with oldhamite
520 exteriors. Red box indicates the area mapped in **figure 4 c and d**.
521
522 **Figure 3.** (**a**) Optical micrograph of a representative polished area of SM41 showing rounded
523 tan-colored olivine similar to SM3 and white grains of calcite in dark fine-grained matrix. (**b**)
524 Calcium map of the area enclosed by the red box shown in (**a**).
525
526 **Figure 4.** Raman spectra collected from the grain highlighted with a red box in **figure 2b**.
527 Spectra from the low- (**a**) and high- (**b**) wavenumber spectral regions are labeled with band
528 assignments discussed in text: ν1 OH stretching, ν2 $Ca(OH)_2$ bending, ν1 C-O stretching of
529 calcite, and disordered carbon (D) and graphite (G). Raman peak amplitude maps (**c** and **d**)
530 highlight two strong portlandite Raman peaks and show its distribution is concentrated within the
531 center of the grain, consistent with elemental distribution maps.

# Figure 1

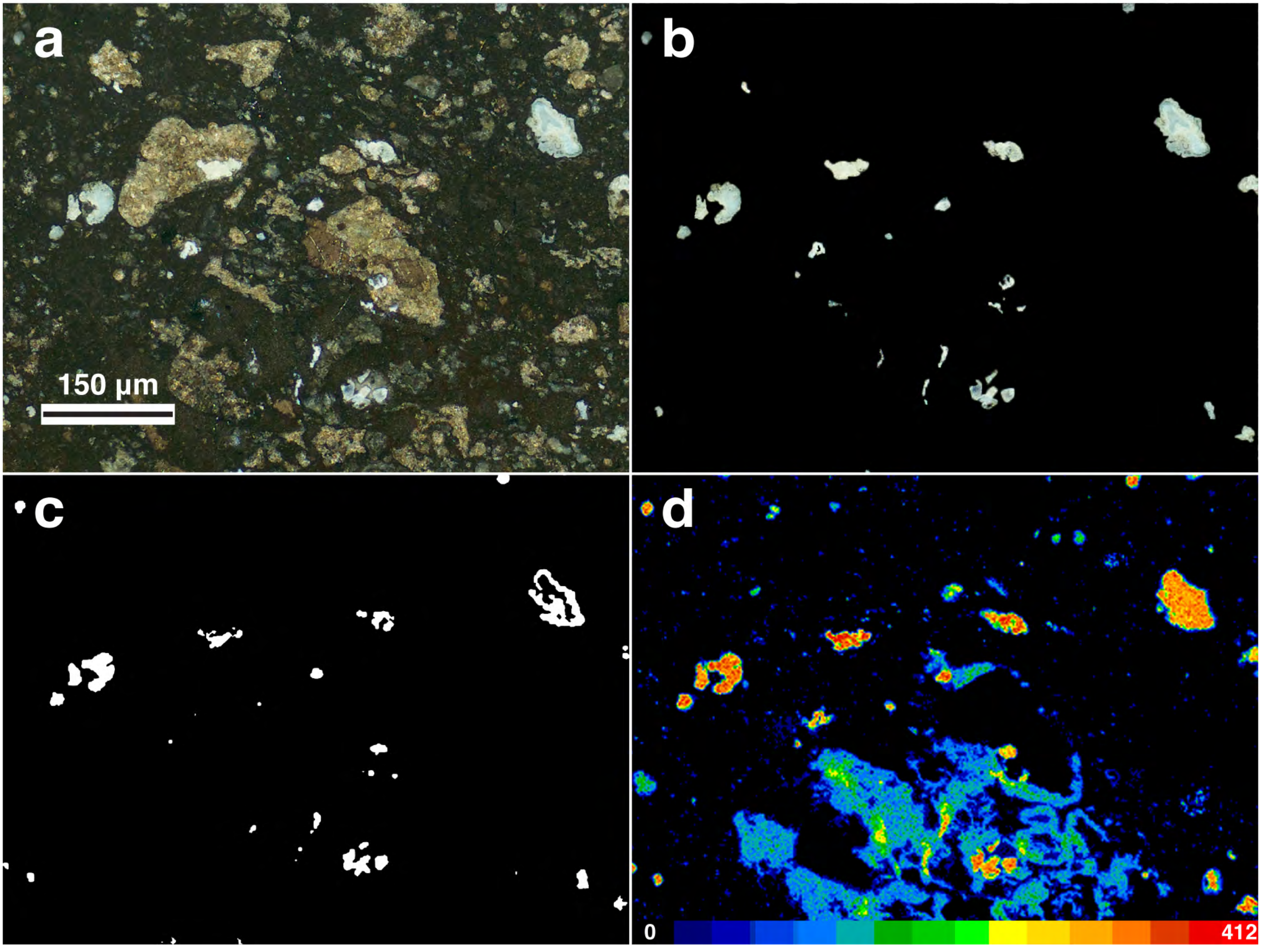

# Figure 2

# Figure 3

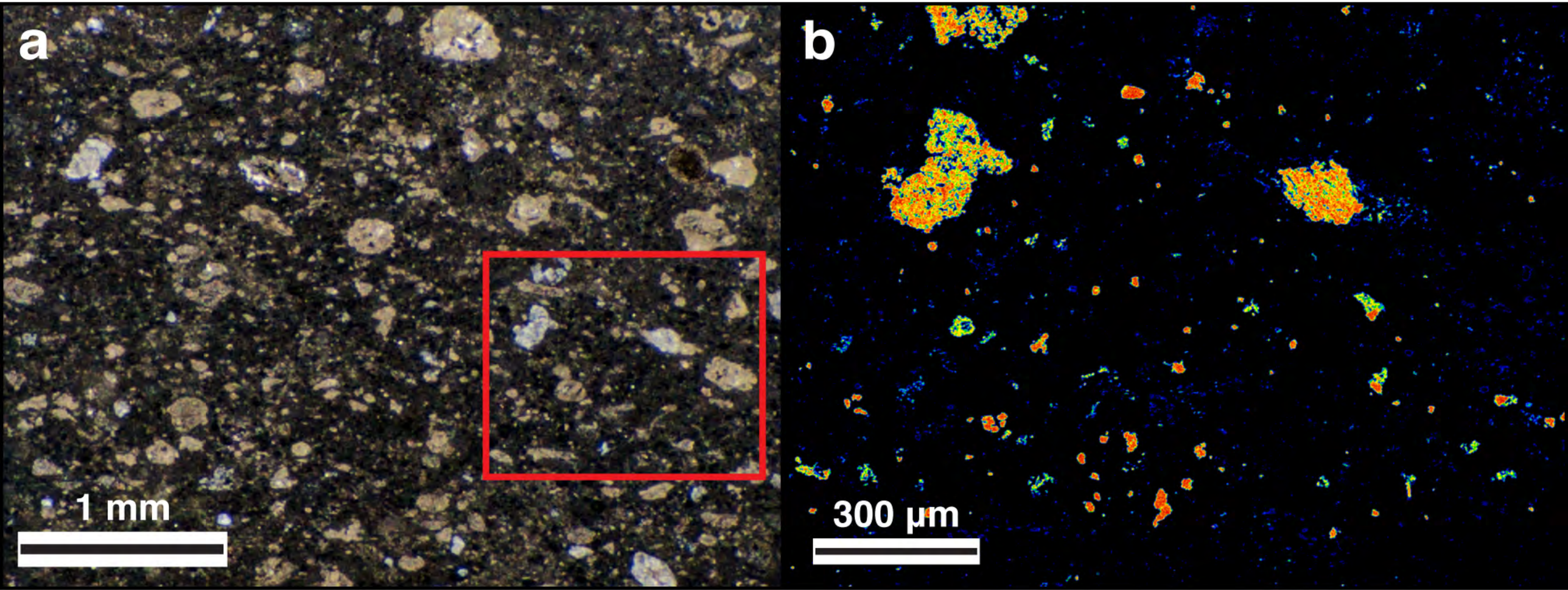

# Figure 4

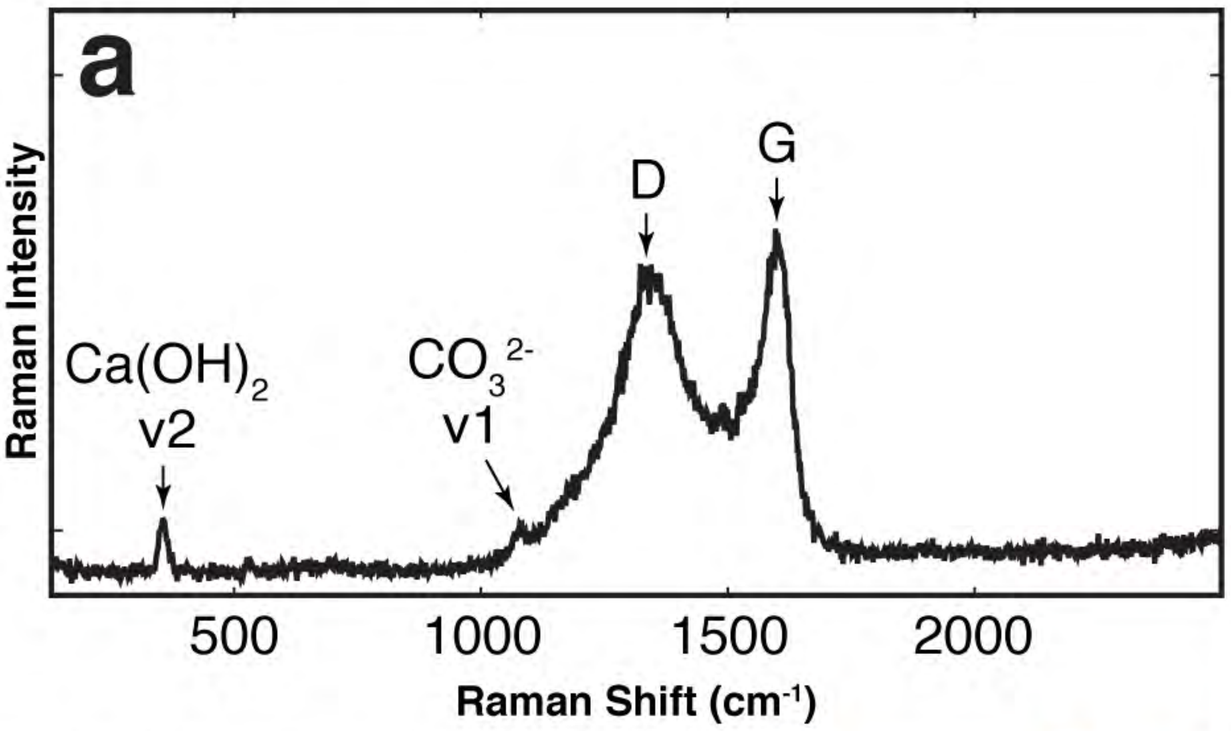
a
Raman Intensity
Ca(OH)2
v2
CO3 2-
v1
D
G
500
1000
1500
2000
Raman Shift (cm-1)

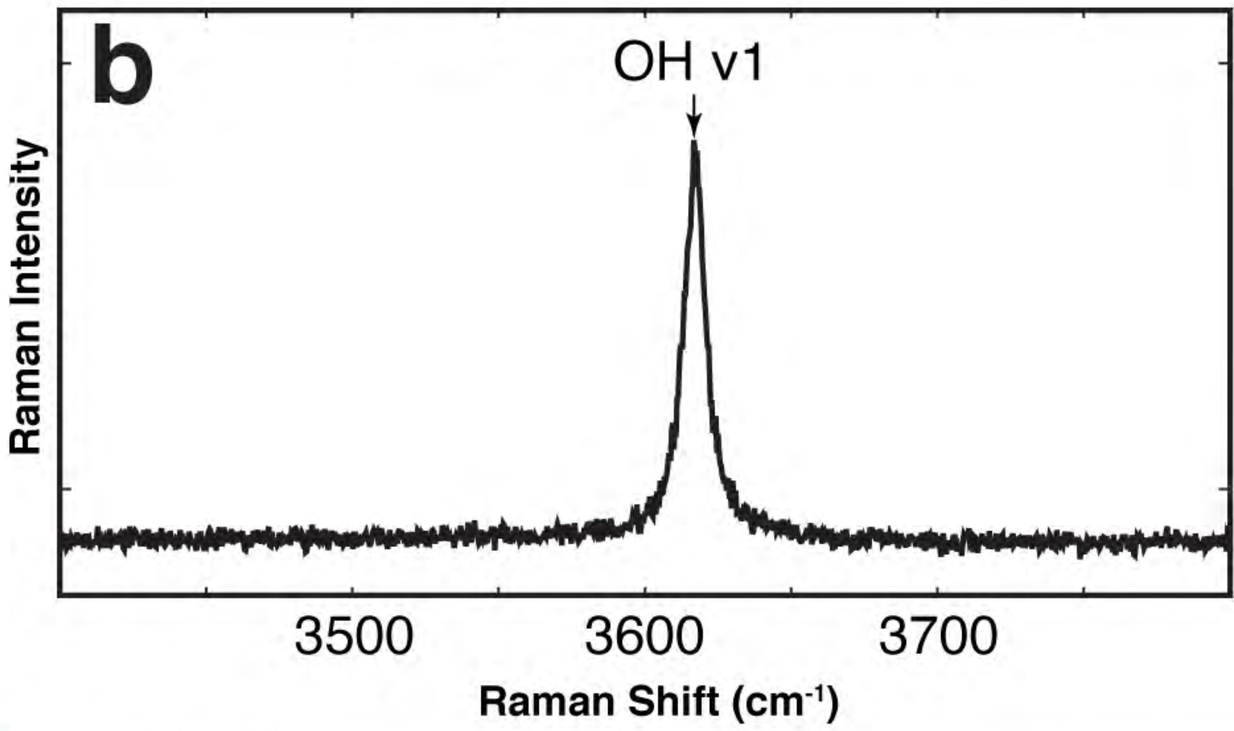
b
Raman Intensity
OH v1
3500
3600
3700
Raman Shift (cm-1)

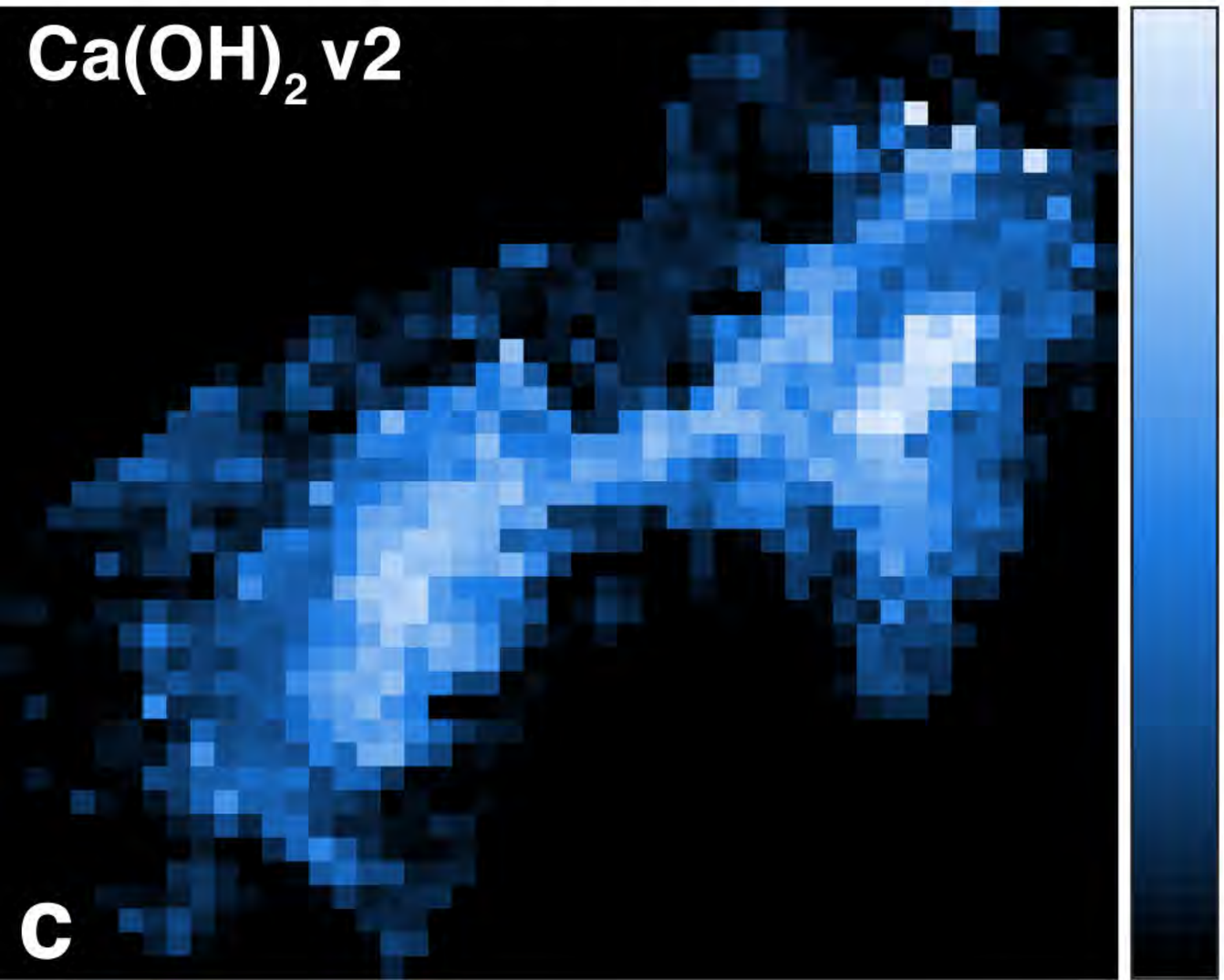
Ca(OH)2 v2
c

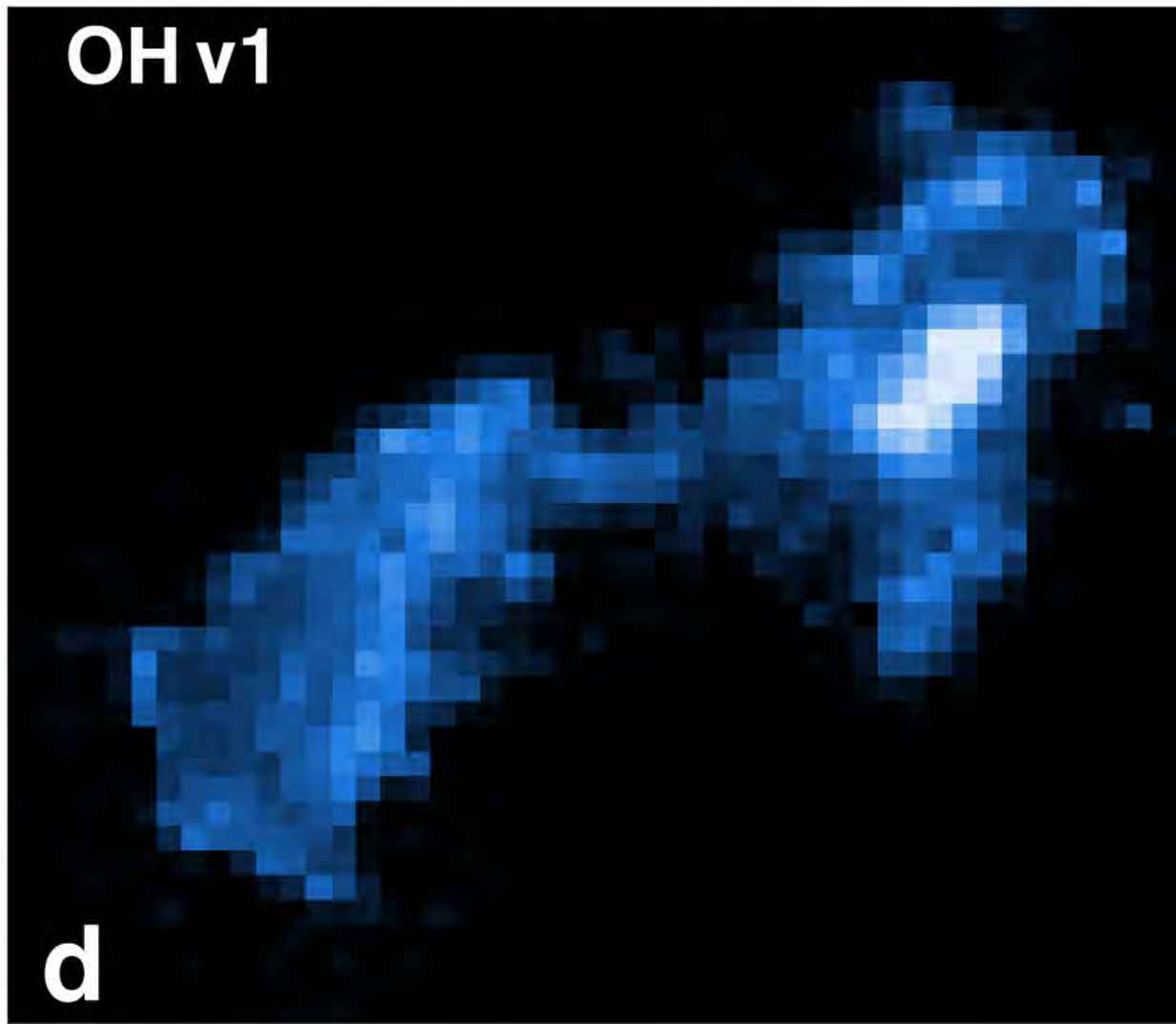
OH v1
d